

1 Ammonium CI-Orbitrap: a tool for characterizing the reactivity
2 of oxygenated organic molecules

3 Dandan Li¹, Dongyu Wang², Lucia Caudillo³, Wiebke Scholz⁴, Mingyi Wang^{5,6}, Sophie Tomaz¹,
4 Guillaume Marie³, Mihnea Surdu², Elias Eccli⁴, Xianda Gong⁷, Loic Gonzalez-Carracedo⁸, Manuel
5 Granzin³, Joschka Pfeifer^{3,9}, Birte Rörup¹⁰, Benjamin Schulze⁶, Pekka Rantala¹⁰, Sébastien Perrier¹,
6 Armin Hansel⁴, Joachim Curtius³, Jasper Kirkby^{3,9}, Neil M. Donahue⁵, Christian George¹, Imad El-
7 Haddad², Matthieu Riva^{1,*}

8 ¹ Univ Lyon, Université Claude Bernard Lyon 1, CNRS, IRCELYON, 69626, Villeurbanne, France

9 ⁶ Institute for Atmospheric and Earth System Research/Physics, Faculty of Science, University of
10 Helsinki, 00014, Helsinki, Finland

11 ² Laboratory of Atmospheric Chemistry, Paul Scherrer Institute, 5232, Villigen, Switzerland

12 ³ Institute for Atmospheric and Environmental Sciences, Goethe University Frankfurt, 60438, Frankfurt
13 am Main, Germany

14 ⁴ Institute for Ion Physics and Applied Physics, University of Innsbruck, 6020, Innsbruck, Austria

15 ⁵ Center for Atmospheric Particle Studies, Carnegie Mellon University, Pittsburgh, PA, 15213, USA

16 ⁶ now at Division of Chemistry and Chemical Engineering, California Institute of Technology, Pasadena,
17 CA 91125, USA

18 ⁷ Leibniz Institute for Tropospheric Research, 04318, Leipzig, Germany

19 ⁸ Faculty of Physics, University of Vienna, Vienna, 1090, Austria

20 ⁹ CERN, the European Organization for Nuclear Research, CH-1211 Geneve 23, Switzerland

21 ¹⁰ Institute for Atmospheric and Earth System Research/Physics, Faculty of Science, University of
22 Helsinki, 00014, Helsinki, Finland

23

24 * Email: matthieu.riva@ircelyon.univ-lyon1.fr

25 Abstract

26 Oxygenated organic molecules (OOMs) play an important role in the formation of atmospheric aerosols.
27 Due to various analytical challenges in measuring organic vapors, uncertainties remain in the formation
28 and fate of OOMs. The chemical ionization Orbitrap mass spectrometer (CI-Orbitrap) has recently been
29 shown to be a powerful technique able to accurately identify gaseous organic compounds due to its great
30 mass resolving power. Here we present the ammonium ion (NH_4^+) based CI-Orbitrap as a technique
31 capable of measuring a wide range of gaseous OOMs. The performance of the NH_4^+ -Orbitrap was
32 compared with that of state-of-the-art mass spectrometers, including a nitrate ion (NO_3^-) based CI
33 coupled to an atmospheric pressure interfaced to long time-of-flight mass spectrometer (APi-LTOF), a
34 new generation of proton transfer reaction-TOF mass spectrometer (PTR3-TOF), and an iodide (I^-)
35 based CI-TOF mass spectrometer equipped with a Filter Inlet for Gases and AEROsols (FIGAERO-
36 CIMS). The instruments were deployed simultaneously in the Cosmic Leaving OUtdoors Droplets
37 (CLOUD) chamber at the European Organization for Nuclear Research (CERN) during the CLOUD14
38 campaign in 2019. Products generated from α -pinene ozonolysis across multiple experimental
39 conditions were simultaneously measured by the mass spectrometers. NH_4^+ -Orbitrap was able to identify
40 the widest range of OOMs (i.e., $\text{O} \geq 2$), from low oxidized species to highly oxygenated organic
41 molecules (HOMs). Excellent agreements were found between the NH_4^+ -Orbitrap and the NO_3^- -LTOF
42 for characterizing HOMs and with the PTR3-TOF for the less oxidized monomeric species. **OOMs**
43 **concentrations measured by NH_4^+ -Orbitrap were estimated using calibration factors derived from the**
44 **OOMs with high timeseries correlations during the side-by-side measurements.** As other mass
45 spectrometry techniques used during this campaign, the detection sensitivity of NH_4^+ -Orbitrap to OOMs
46 is greatly affected by relative humidity, which may be related to changes in ionization efficiency and/or
47 multiphase chemistry. Overall, this study shows that NH_4^+ ion-based chemistry associated with the high
48 mass resolving power of the Orbitrap mass analyzer can measure almost all-inclusive compounds. As a
49 result, it is now possible to cover the entire range of compounds, which can lead to a better understanding
50 of the oxidation processes.

51

52 **1 Introduction**

53 Aerosols affect the climate by either directly scattering or absorbing solar radiation, or acting as seeds
54 for cloud formation (Fan et al., 2016; Haywood and Boucher, 2000). A major fraction of submicron
55 aerosol mass consists of organic compounds, with secondary organic aerosol (SOA) predominating
56 (Jimenez et al., 2009; Hallquist et al., 2009). Oxygenated organic molecules (OOMs) generated from
57 the oxidation of volatile organic compounds (VOCs) contribute to the formation and growth of SOA
58 (Ehn et al., 2014; Mellouki et al., 2015). OOMs can be generated through bimolecular peroxy radicals
59 (RO_2) pathway or by the autoxidation of RO_2 followed by the termination pathways (Bianchi et al., 2019;
60 Mohr et al., 2019). Among the OOMs, the highly oxygenated organic molecules (HOMs), containing
61 multiple functional groups and exhibiting (extremely) low saturation vapor pressure, can nucleate in
62 concert with inorganic species e.g., sulfuric acid or on their own (Ehn et al., 2014; Kirkby et al., 2016;
63 Bianchi et al., 2016), forming new particles. Less oxygenated molecules (i.e., containing 2 to 5 oxygen
64 atoms) play a vital role in the growth of newly formed atmospheric particles, either by condensation or
65 through multiphase chemistry (Bianchi et al., 2019; Ehn et al., 2014; Hallquist et al., 2009). Therefore,
66 the identification and quantification of the wide diversity of OOMs are essential to understand SOA
67 formation and growth (Kirkby et al., 2016; Bianchi et al., 2016; Ehn et al., 2014).

68 Mass spectrometry (MS) has made remarkable achievements in detecting, characterizing, and
69 quantifying OOMs (Wang et al., 2020; Breitenlechner et al., 2017; Bianchi et al., 2019; Ehn et al., 2010;
70 Riva et al., 2019a). Moreover, the application of chemical ionization (CI) enables the detection of a wide
71 variety of organic and inorganic analytes (Bianchi et al., 2019; Ehn et al., 2014; Jokinen et al., 2012;
72 Lee et al., 2014). However, the selection of ionization chemistry in combination with MS detection
73 technique will impact the methods selectivity and sensitivity toward certain groups of OOMs (Bianchi
74 et al., 2019; Riva et al., 2020; Riva et al., 2019b; Berndt et al., 2018b; Berndt et al., 2018a). For example,
75 negative ion-based chemistry, including nitrate (NO_3^-), can optimally detect HOMs, which only
76 constitute a small subset of the OOMs (Lee et al., 2014; Berndt et al., 2018b; Riva et al., 2019b); iodide
77 (I^-) can efficiently detect various OOMs with 3-5 oxygen atoms (Riva et al., 2019b; Lee et al., 2014).
78 Positive ion-based chemistries have also been developed, showing great sensitivity to HOMs as well as
79 less oxidized products, providing the possibility of achieving carbon closure of the OOMs (Berndt et al.,
80 2018a; Berndt et al., 2018b; Hansel et al., 2018; Riva et al., 2020; Riva et al., 2019b). However, these
81 positive ion methods are mainly based on proton transfer and often result in fragmentation of the analytes
82 (Breitenlechner et al., 2017). Time-of-flight (TOF) mass spectrometers using ammonium (NH_4^+) or
83 amines as reagent ions can detect a wide variety of OOMs but suffer from a lack of mass resolving
84 power, making peak identification challenging, especially for complex systems, i.e., under ambient
85 conditions (Berndt et al., 2018b; Berndt et al., 2018a; Riva et al., 2019b). Finally, the recently developed
86 Orbitrap mass spectrometer using propylamine has achieved unambiguous identification of overlapping
87 peaks and accurate quantification of OOMs (Riva et al., 2020). However, this analytical technique has
88 been used in very diluted and dry environments to ensure a linear response to the OOMs produced from
89 simple atmospheric systems, i.e., a single VOC precursor and oxidant (Riva et al., 2020; Riva et al.,
90 2019b).

91 Here, we explore the capability of NH_4^+ ion-based CI-Orbitrap mass spectrometer (Q-Exactive
92 Orbitrap, Thermo Scientific) for detecting OOMs generated from α -pinene ozonolysis in the Cosmic
93 Leaving OUTdoors Droplets (CLOUD) chamber at the European Organization for Nuclear Research
94 (CERN) under various environmental conditions. We compare the performance of the NH_4^+ -Orbitrap to
95 state-of-the-art online mass spectrometers including a nitrate CI atmospheric pressure interface long
96 time of flight mass spectrometer (NO_3^- -LTOF; Tofwerk AG), a proton transfer reaction time of flight
97 mass spectrometer (PTR3-TOF; Ionicon Analytik GmbH), and gas phase of an iodide CI time of flight
98 mass spectrometer equipped with a Filter Inlet for Gases and AEROsols (I⁻-CIMS, Tofwerk AG).

99 **2 Experimental approach and product analysis**

100 **2.1 CLOUD chamber experiments**

101 All experiments were conducted in the CLOUD chamber, a 26 m³ cylindrical stainless-steel vessel at
102 CERN. The chamber can achieve a pristine background for the study of nucleation (Kirkby et al., 2016).
103 The chamber operated as a continuously stirred tank reactor (CSTR), with mixing driven by two
104 inductively coupled fans at the top and bottom of the chamber. Evaporated liquid nitrogen (N₂) and
105 liquid oxygen (O₂) were blended at a ratio of 79:21 to provide ultra-pure synthetic air, which flushed
106 the chamber constantly. Variable amounts of trace gases, including O₃, VOCs, NO_x, SO₂, and CO were
107 accurately injected into the chamber via a gas control system and monitored. Photolysis was driven by
108 various light sources, including Hg-Xe UV lamps, and UV excimer laser. Between experiments, the
109 chamber was cleaned by irrigating the walls with ultra-pure water, then heated to 373 K, and flushed
110 with humidified pure air and high ozone, reducing the contaminant (e.g., VOCs) to sub pptv levels.
111 During the cleaning process, particles were removed using a high-voltage electric field.

112 The results presented here were from the CLOUD14 campaign performed in autumn 2019. During
113 CLOUD14, the total flow was kept at 250 standard liters per minute (slpm), providing an average
114 residence time of 104 minutes. α -Pinene was introduced into the chamber by passing a small flow of
115 dry air over a temperature-controlled evaporator containing liquid α -pinene. Ozone was generated by
116 flowing a small fraction of the air through a quartz tube surrounded by UVC lights (wavelength < 240
117 nm). Experiments were performed at low temperature (263 \pm 0.1 K). The RH in the chamber was
118 controlled by flowing a portion of the air through a Nafion® humidifier using ultrapure water (18 M Ω
119 cm, Millipore Corporation). The contents of the chamber were monitored by a wide range of external
120 instruments connected to the sampling probes that protrude \sim 1 m into the chamber.

121 **2.2 Product analysis by NH_4^+ -Orbitrap**

122 The chemical composition of closed-shell molecules was determined in real time by means of a CI-
123 Orbitrap sampling from the CLOUD chamber through a 750 mm long, 10 mm inner diameter Teflon
124 tube at a flow rate of 10 slpm. The CI inlet mounted on the Orbitrap was custom-built with minor
125 modifications from the commercial inlet (Riva et al., 2019a). The ion-molecule reaction (IMR)
126 proceeded at atmospheric pressure with a residence time of 200-300 ms. The same operating parameters
127 used in our previous studies (RF level 60, automatic gain control 1×10^6 charges, maximum injection

128 time 1000 ms, multi RF ratio 1.2, mass resolution $m/\Delta m$ 140,000 at m/z 200), were used, thereby
129 minimizing declustering and maximizing the linearity range (Riva et al., 2019a; Riva et al., 2020; Cai
130 et al., 2022).

131 The high resolution Orbitrap mass spectra data were analyzed using “Orbitool” software with a
132 graphical user interface (GUI) (<https://orbitrap.catalyse.cnrs.fr>) (Cai et al., 2021). The analysis
133 procedures included data averaging, noise determination and reduction, single peak fitting, mass
134 calibration, assignment of molecular formulas, and export of time series. Signals were averaged over 5
135 min before determining the noise and performing mass calibration.

136 NH_4^+ has been utilized in PTR-MS with a low pressure (Berndt et al., 2018b; Hansel et al., 2018).
137 Here, this ionization technique was used to detect OOMs in atmospheric pressure and was operated in a
138 similar fashion as in our initial study (Riva et al., 2019a). NH_3 was added into the ion source by flushing
139 2 sccm of dry air over the headspace of a 1% liquid ammonia water mixture (prepared from a MilliQ
140 water and a 25% ammonium hydroxide stock solution, ACS reagent, Sigma-Aldrich). The product
141 molecules (“prod”) were softly charged by binding to ammonium (NH_4^+) ions, forming (prod)- NH_4^+
142 adduct ions or protonated products (prod)- H^+ , following either reaction (1) or (2),



145 The NH_4^+ reagent ion cannot be directly detected due to the cut-off of the Orbitrap mass analyzer
146 (i.e., m/Q 50). Hence, normalization of the raw analyte signals is difficult and hinders quantification of
147 OOMs. However, we observed a total of 62 peaks corresponding to amines, including $\text{C}_4\text{H}_{12}\text{N}^+$, and
148 $\text{C}_6\text{H}_{14}\text{N}^+$, which are formally ammonia derivatives. To some extent, their signals can be used to correct
149 for changes in NH_4^+ ion chemistry. Among these peaks, 13 were abundant and constant throughout the
150 measurement period (Fig. S1). As a result, these signals were used as surrogates for the primary reagent
151 ions to normalize the signal intensity of the OOMs (equation 3) and to account for the potential variation
152 of the ionization process (Riva et al., 2019b).

153
$$[\text{OOM}]_{\text{nor}} = \frac{[(\text{OOM})\text{-NH}_4^+] + [(\text{OOM-}\text{H})^+]}{\sum[\text{Amine}]} \quad (3)$$

154 Correlation analysis were performed between the NH_4^+ -Orbitrap and the two reference
155 instruments including NO_3^- -LTOF and PTR3-TOF (referred to as REF). The Pearson correlation
156 coefficients (R^2) were determined using the timeseries during two runs (run 2211 and 2213). This
157 included AP injection, steady state stage, NO_x or CO injections, and RH variation. As a result, for one
158 compound, 755 data points were recorded and used for the correlation analysis. Although product ions
159 with same molecular formulas might lead to low correlation (See details in section 3.3) and would
160 suggest different species (i.e., isomers, fragment ions,...), a few molecules with R^2 greater than 0.9 (18
161 for NO_3^- -LTOF, 32 for PTR-TOF, and 5 for I^- -CIMS) were selected and be likely attributed to the same
162 species.

163 Although no direct calibration has been performed for the NH_4^+ -Orbitrap, the OOM
164 concentrations were estimated based on comparisons between NH_4^+ -Orbitrap and the two reference
165 instruments which has developed reliable quantification methods. For the OOMs whose timeseries had
166 R^2 greater than 0.9 between NH_4^+ -Orbitrap and REF, linear regression was conducted for normalized
167 intensities in NH_4^+ -Orbitrap (dimensionless) and concentrations in REF (molecules cm^{-3}), and the slopes
168 were recorded as their relative sensitivity. The calibration factor $c_{\text{Orbi-REF}}$ was derived from the
169 averaged relative sensitivity of these species ($\sim 2.62 \times 10^8$ molecules cm^{-3} for NO_3^- -LTOF and $\sim 4.83 \times$
170 10^8 molecules cm^{-3} for PTR3-TOF). Applying the calibration factors to all the OOMs, their
171 concentrations detected by NH_4^+ -Orbitrap could be calculated as shown in equation (4). Additionally, a
172 temperature-dependent sampling-line loss correction factor was applied (Simon et al., 2020).

173
$$[\text{OOM}]_{\text{Orbi-REF}} = c_{\text{Orbi-REF}} \times [\text{OOM}]_{\text{nor}} \quad (4)$$

174 **2.3 Product analysis by NO_3^- -LTOF**

175 Detection of RO_2 radicals and closed-shell products was also performed by the NO_3^- -LTOF which has
176 been described elsewhere (Jokinen et al., 2012; Caudillo et al., 2021). Therefore, only relevant details
177 for this study are provided here. The NO_3^- -LTOF used in this study had a mass resolving power of $m/\Delta m$
178 12,000 and detected OOMs (mass 300-650 Da) as clusters ions with $(\text{HNO}_3)_n(\text{NO}_3^-)$ anions, with $n = 0$ -
179 2. The limit of detection (LoD) for OOMs is 5×10^4 molecules cm^{-3} (Simon et al., 2020). The primary
180 ions were produced by a corona discharge needle exposed to a sheath gas enriched by HNO_3 . Laminar
181 flow diffusional loss was assumed in the 30 cm sampling line. A core-sampling technique was applied ,
182 which drew a core flow of 5.1 slpm from the center of a 30 slpm total flow. This setup reduced the
183 sampling loss rate of HOMs to less than 30% (Simon et al., 2020).

184 The data were processed using Tofware (Version 3.2, Aerodyne Inc., USA) and MATLAB R2019b
185 (MathWorks, Inc., USA). In addition, background signals, mass-dependent transmission efficiency
186 (Heinritzi et al., 2016), and sampling losses (Simon et al., 2020) were determined and corrections were
187 applied. The NO_3^- -LTOF was directly calibrated using sulfuric acid (H_2SO_4), where the detection
188 efficiency of HOMs was assumed as similar to H_2SO_4 . However, OOMs with less oxygen number (O
189 < 6) were prone to a lower detection efficiency compared to H_2SO_4 , leading to an underestimation
190 (Stolzenburg et al., 2018; Ehn et al., 2014). A calibration factor C was determined to be $\sim 4.13 \times 10^{10}$
191 molecules cm^{-3} during CLOUD14 (Caudillo et al., 2021). The concentration of OOMs was also
192 corrected using a mass dependent transmission efficiency inferred by depleting the reagent ions with
193 several perfluorinated acids. Assuming that OOMs got lost in sampling lines due to diffusion, the losses
194 of OOMs were corrected with a diffusion coefficient scaling with the molecular mass. More information
195 could be found in former studies (Heinritzi et al., 2016; Stolzenburg et al., 2018; Simon et al., 2020;
196 Caudillo et al., 2021).

197 **2.4 Product analysis by PTR3-TOF**

198 The PTR3-TOF ionizes organic compounds by proton transfer or ligand swith reactions where
199 protonated water clusters $(\text{H}_2\text{O})_n\text{H}_3\text{O}^+$ with $n=1-3$ were produced by a corona discharge using

humidified nitrogen (Breitenlechner et al., 2017). To reduce sample losses, a 2 slpm was drawn from a 10 slpm laminar flow through a critical orifice into the tripole where the ion-molecule reactions occur. The pressure in this region was maintained at \sim 80 mbar. The distribution of primary ions and sample molecules can be adjusted by a tunable radio frequency signal applied to the tripole rods. The LoD of PTR3-TOF for detecting OOMs is 8×10^5 molecules cm^{-3} (Breitenlechner et al., 2017).

During the CLOUD14 experiments, the collision energy was controlled between 62 and 72 Td to reduce the methods humidity dependence which may complicate the detection of organic compounds. A gas standard mixture containing 1 ppm of 3-hexanone, heptanone, and α -pinene in nitrogen was dynamically diluted by a factor of 1000 in VOC-free air to contain 1 ppbv of each compound, and then was used to calibrate the PTR3-TOF. All data were analyzed using TOF-Tracer software running on Julia 0.6 (<https://github.com/lukasfischer83/TOF-Tracer>) and were further corrected for the duty cycle transmission of TOF and temperature dependent sampling line losses (Stolzenburg et al., 2018). On the one hand, duty cycle corrected counts per second dcps , $\text{dcps}_i = \text{cps}_i \times (101/m_i)^{1/2}$, was utilized to account for the mass-dependent transmission of the TOF mass spectrometer (Breitenlechner et al., 2017). The calculated sensitivities of 3-hexanone and heptanone were comparable to the observed ones. Therefore, the concentration of oxygenated products was estimated using the sensitivity of 3-hexanone as lower-limit values due to possible fragmentation (Breitenlechner et al., 2017; Stolzenburg et al., 2018). On the other hand, the detected OOMs having (extremely) low volatility were assumed to be lost by diffusion and adjusted by a temperature dependent loss-correction. The sampling line losses considered three loss sections under different temperatures, including losses at the sampling lines within and outside the chamber and within the PTR3-TOF instrument. Details can be found in previous studies (Breitenlechner et al., 2017; Stolzenburg et al., 2018).

2.5 Product analysis by I⁻-CIMS

The I⁻-CIMS was capable of characterizing both gas and particle phases (Lopez-Hilfiker et al., 2014). In the gas-phase mode, gases were directly sampled into a 100-mbar turbulent ion-molecule reactor, while particles were collected onto a polytetrafluoroethylene (PTFE) filter through a separate dedicated sampling port. Analytes were then ionized with I⁻ chemical ionization and extracted into a TOF mass analyzer (Wang et al., 2020). The LoD of I⁻-CIMS for OOMs could be lower to \sim 10⁷ molecules cm^{-3} (Lee et al., 2014). In this study, only gas phase data are reported.

Iodide ions (I⁻) were used as the reagent ions and formed by passing a 1.0 slpm flow of ultrahigh purity N₂ over a diffusion tube filled with methyl iodide (CH₃I), and then through a ²¹⁰Po radioactive source. In the sampling mode, the reagent ion flow was mixed with a sample flow in the IMR at \sim 150 mbar. Coaxial core sampling was used to minimize the vapor wall loss in the sampling line. The total flow was kept at 18.0 slpm and the core flow at 4.5 slpm; the instrument sampled at the center of the core flow with a flow rate of 1.6 slpm. The gas-phase background signal was determined by routinely introducing zero air directly into the inlet. Data were analyzed using Tofware (2.5.11_FIGAERO version; Aerodyne Inc., USA) giving 10 s average mass spectra. The ion signal was normalized by the sum of reagent ion signals (i.e., m/Q 127: I⁻ and 145: H₂OI⁻).

238 **2.6 Volatility of OOMs**

239 It is challenging to directly measure the vapor pressure of individual OOMs due to the difficulty to
 240 acquire authentic standards. To overcome experimental challenges, model calculations have been
 241 developed to estimate the vapor pressure using, for example, structure-based estimations and formula-
 242 based estimations (Pankow and Asher, 2008). Volatility basis set (VBS), a categorization framework
 243 based on quantifiable organic property (i.e., volatility) has been established and is frequently used to
 244 characterize oxidation chemistry (Donahue et al., 2011; Li et al., 2016). The VBS parameterization is
 245 useful for classifying the wide range of OOMs into multiple volatility groups, including extremely low
 246 volatility organic compounds (ELVOC) and low volatility organic compounds (LVOC) based on their
 247 effective saturation concentration (C^*) in the unit of $\mu\text{g m}^{-3}$ (Bianchi et al., 2019). In this study, we
 248 applied the VBS parameterization optimized by Li et al (Li et al., 2016; Isaacman-Vanwertz and Aumont,
 249 2021).

$$250 \quad \log_{10}C^*(298K) = (n_C^0 - n_C)b_C - n_Ob_O - 2\frac{n_Cn_O}{(n_C+n_O)}b_{CO} - n_Nb_N - n_Sb_S \quad (5)$$

251 where n_C , n_O , n_N , and n_S was the number of carbon, oxygen, nitrogen, and sulfur atoms of the specific
 252 molecule, separately; n_C^0 was the reference carbon number; b_C , b_O , b_N , and b_S was the contribution of
 253 each atom to $\log_{10}C^*$, respectively; b_{CO} was the carbon-oxygen nonideality (Donahue et al., 2011).
 254 Values of b coefficient can be found in Li et al.(Li et al., 2016). The formula used to estimate the vapor
 255 pressure was amended to convert all NO_3 groups into OH groups to reduce the bias from the compounds
 256 containing nitrates (Daumit et al., 2013; Isaacman-Vanwertz and Aumont, 2021).

257 Due to the different temperatures in the CLOUD14 experiments, we adjusted $C^*(298K)$ to the
 258 measured experimental temperature in equations (6) and (7):

$$259 \quad \log_{10}C^*(T) = \log_{10}C^*(298K) + \frac{\Delta H_{vap}}{R\ln(10)} \times \left(\frac{1}{298} - \frac{1}{T}\right) \quad (6)$$

$$260 \quad \Delta H_{vap}(\text{kJ mol}^{-1}) = -11 \cdot \log_{10}C^*(298K) + 129 \quad (7)$$

261 where T was the temperature in Kelvin, $C^*(298K)$ was the saturation vapor concentration at 298 K,
 262 ΔH_{vap} was the evaporation enthalpy and R was the gas constant ($8.3134 \text{ J K}^{-1} \text{ mol}^{-1}$). The potential
 263 presence of isomers may result in uncertainty in this method since the only input is the compound's
 264 molecular formula.

265 In this study, all oxidation products were grouped into six volatility regimes; ultralow-volatility
 266 (ULVOCs, $C^* < 10^{-8.5} \mu\text{g m}^{-3}$), extremely low volatility (ELVOCs, $10^{-8.5} < C^* < 10^{-4.5} \mu\text{g m}^{-3}$), low-
 267 volatility (LVOCs, $10^{-4.5} < C^* < 10^{-0.5} \mu\text{g m}^{-3}$), semi-volatile (SVOCs, $10^{-0.5} < C^* < 10^{2.5} \mu\text{g m}^{-3}$),
 268 intermediate-volatility organic compounds (IVOC, $10^{2.5} < C^* < 10^{6.5} \mu\text{g m}^{-3}$), and VOC ($10^{6.5} < C^* \mu\text{g}$
 269 m^{-3}) based on VBS.

270 **3 Results and Discussions**

271 **3.1 Peak identification of NH₄⁺-Orbitrap**

272 As a promising reagent ion for detecting the full range of OOMs, more ions with low concentration were
273 captured by NH₄⁺, whose identification and quantification were most affected by overlapping signals.
274 The relative intensities of neighboring peaks should also be considered when estimating their ease of
275 separation. It has been shown that the higher mass resolution reduced the interference of adjacent peaks
276 based on NO₃⁻ or C₂H₃O₂⁻ reagent ions (Riva et al., 2019a; Riva et al., 2020). Therefore, the ability of
277 the NH₄⁺-Orbitrap for separating overlapping mass spectral peaks was compared to NH₄⁺-TOF.

278 The mass resolving power was defined as the ratio of m to Δm , where m was the mass-to-charge
279 ratio of the analyte ion, and Δm was the full width at half maximum (FWHM). Higher mass resolving
280 power allows unambiguous mass spectral peak assignment. For a pair of overlapping peaks of equal
281 intensity, the distance between their respective peak center, referred to hereafter simply as peak distance,
282 dm , needed to be greater than approximately 0.8 of the FWHM of the overlapping peaks, such that they
283 could be reasonably deconvolved as shown in Fig. S2. Depending on their experience, individuals may
284 be able to visually identify the presence of overlapping peaks at lower or higher dm values. We
285 arbitrarily defined the minimum dm (normalized to that of FWHM, or Δm) as the value at which the
286 observed spectrum (“Combined” trace in Fig. S2 and S3) had a local minimum between the centers of
287 the overlapping peaks (i.e., there was a “dip” in the observed signal between ion peaks). The minimum
288 dm value increased with the intensity ratio of overlapping peaks, ranging roughly from 0.85 (for equally
289 intense peaks) to 1.43 (for peaks differing one order of magnitude in their respective intensities), as
290 shown in Fig. S3. In practice, noise and the presence of additional neighboring peaks would further
291 complicate peak deconvolution. For simplicity, we used a normalized dm of 1 (i.e., $dm = \Delta m$) as a
292 threshold for unambiguous deconvolution of neighboring peaks.

293 Figure 1 shows the histogram of the distances between neighboring peaks normalized against the
294 FWHM for the NH₄⁺-Orbitrap and the NH₄⁺-TOF having a mass resolving power of 10,000. In each
295 histogram, one count indicated that an ion had at least one neighboring ion with a relative intensity of
296 20%, 50%, or 100% (with a higher relative intensity threshold value being less selective). Neighboring
297 ions separated by distances exceeding 2 times the FWHM were considered well-separated. For ions with
298 multiple neighboring peaks within the 2 x FWHM separation distance window, the distance to the first
299 neighboring peak that satisfied the aforementioned relative intensity threshold was reported. Overall,
300 NH₄⁺-Orbitrap can separate most of the observed ions (> 99%), while the NH₄⁺-TOF, depending on the
301 relative intensity threshold set, can separate only 32% to 46% of all the ions by at least 1 FWHM. It
302 should be noted that the NH₄⁺-Orbitrap has shown its strength in separating neighboring peaks in
303 controlled experiments, in which the knowledge of the chemical compositions for OOMs is relatively
304 abundant. The advantages of higher mass resolving power should be further stressed in ambient
305 observations, where the knowledge about OOM species can be limited with a larger number of
306 detectable peaks.

307

308 **3.2 Characterization of OOMs by four instruments**

309 Illustrated in Fig. 2 are mass defect plots of OOMs measured by NH_4^+ -Orbitrap, NO_3^- -LTOF, PTR3-
310 TOF, and I^- -CIMS, identifying species of 484, 252, 145, and 67, respectively in run 2211. The NH_4^+ -
311 Orbitrap detected the widest range of products, including HOMs and the less oxidized species (i.e., O <
312 6). Out of the 484 compounds, 5% were amines. The number of O atoms in OOMs varied from 1 to 11
313 in monomers (C_{2-10}) and from 2 to 16 for dimeric products (C_{14-20}), with an average elemental oxygen-
314 to-carbon ratio (O:C) of 0.4 ± 0.2 (the value following “ \pm ” herein and after refers to the standard
315 deviation of O:C during the experiment). As expected, the NO_3^- -LTOF exhibited a very good sensitivity
316 towards HOMs, with the highest O:C of 0.7 ± 0.3 . The PTR3-TOF mainly detected compounds below
317 m/Q 300 Th with an average O:C of 0.5 ± 0.3 , which was due to the optimization to (i.e., lowering E/N
318 value) measure ammonia and amines sensitively, which ultimately impacted its capability to detect
319 efficiently OOMs. However, many less oxygenated OOMs were still observed by the PTR3-TOF and
320 were used to conduct the correlation analysis of time series with those detected by the NH_4^+ -Orbitrap.
321 Due to the selectivity and potential losses within the sampling line/inlet of the I^- -CIMS equipped with
322 a FIGAERO inlet fewer monomers of C_{8-10} and dimers of C_{19-20} were observed, with an average O:C of
323 0.5 ± 0.2 .

324 **3.3 Instrumental comparisons: correlations**

325 Due to differences in selectivity and sensitivity of the analytical methods toward OOMs, ~42% of the
326 identified species by NH_4^+ -Orbitrap are simultaneously detected by other mass spectrometers (Fig. S4).
327 To identify how NH_4^+ -Orbitrap performed compared to the other mass spectrometers, a correlation
328 analysis including all co-detected ions was complied. The experimental conditions of the runs used for
329 performing this analysis are summarized in Table S1. The data set covered a variety of conditions, such
330 as different concentrations of α -pinene, NO_x , SO_2 , and CO, as well as RH. R^2 was calculated, using the
331 time series of OOMs having the same elemental composition measured by the different mass
332 spectrometers. Figure 3 displays the correlation coefficient of time series for the detected compounds,
333 with marker size scaled by R^2 . The NH_4^+ -Orbitrap and the NO_3^- -LTOF detected OOMs with the same
334 chemical compositions, covering monomers and dimers, among which 18 OOMs showed $R^2 > 0.9$.
335 Regarding the PTR3-TOF, the NH_4^+ -Orbitrap demonstrated high correlations for most of the monomers
336 and fewer dimers, including 32 species having an $R^2 > 0.9$. Due to potential losses within the FIGAERO
337 inlet, fewer OOMs were detected by the I^- -CIMS. However, certain families of compounds, including
338 $\text{C}_{10}\text{H}_{15}\text{O}_{5.7}\text{N}$ and $\text{C}_{20}\text{H}_{31}\text{O}_{7.9}\text{N}$ showed high correlations (i.e., $R^2 > 0.9$) between the NH_4^+ -Orbitrap and
339 with the I^- -CIMS. Finally, the NO_3^- -LTOF was regarded as the reference instrument for HOMs
340 measurements. Only fewer monomers with high oxygen content were detected by the NO_3^- -LTOF and
341 the PTR3-TOF, and only a few dimers between the NO_3^- -LTOF and the I^- -CIMS with moderate
342 relevance.

343 The reason why the correlations of certain molecules are lower than 0.9 might be due to the
344 molecules' composition or potential ionization artifacts. RH dependence is an important property
345 leading to the low correlations as the experiment includes RH variation from 20% to 80%. Although

346 NO_3^- ion chemistry had been reported to be less dependent on RH (Viggiano et al., 1997), the
347 sensitivities of PTR3-TOF (Breitenlechner et al., 2017) and I^- -CIMS (Lee et al., 2014) both showed
348 high dependence on RH. In addition, the relative sensitivity of NH_4^+ -Orbitrap was also influenced by
349 the varying RH (See details in Section 3.6). Fragmentation, such as decomposition of dimers, would
350 also lead to low correlations. However, less fragmentation is expected to occur in the NH_4^+ -Orbitrap
351 using similar settings as our earlier studies (Riva et al., 2019a; Riva et al., 2020). In comparison,
352 decomposition of peroxides (i.e., ROOR and ROOH) can be expected within the PTR3-TOF. While
353 fragmentation of dimeric compounds can contribute to the overall signal of the monomers, the
354 concentration of such species remains minor (Li et al., 2022). As a result, no large enhancement of the
355 monomers signal intensity is expected. There are also other artifacts which cannot be excluded based on
356 current dataset, including potential isomers and differences in response time between instruments, would
357 also lead to the low correlations. However, by comparing the coverage regions of the instruments across
358 multiple experimental conditions, the NH_4^+ -Orbitrap was capable of covering the widest range of
359 compounds and showed an overall good agreement with other mass spectrometers.

360 **3.4 Instrumental comparisons: concentration estimates**

361 Concentrations of the identified compounds were estimated for NH_4^+ -Orbitrap, as described in section
362 2.2. The sensitivity of NH_4^+ -Orbitrap was constrained based on the intensity comparison between NH_4^+ -
363 Orbitrap and the other two instruments. For instance, concentrations of the most abundant C_{10} -
364 monomers (i.e., $\text{C}_{10}\text{H}_{14/16}\text{O}_n$) were estimated using different calibration factors (Fig. 4), which were
365 measured during steady-state conditions (i.e., Run 2211 with $[\text{O}_3] = 100$ ppbv and $[\alpha\text{-pinene}] = 2$ ppbv,
366 $\text{RH} = 10\%$). The concentrations of C_{10} -monomers measured by the NH_4^+ -Orbitrap based on the two
367 calibration factors vary within a factor of 2, which indicates the consistency between the two correlation
368 analyses. The variation trend of concentrations with the oxygen number of the NH_4^+ -Orbitrap is similar
369 to that of the NO_3^- -LTOF in the range of $n_{\text{O}} > 6$, and it is similar to that of the PTR3-TOF in the range of
370 $n_{\text{O}} = 1 \sim 5$. Taking into consideration that such ranges are also the oxygen number ranges with high
371 sensitivities respectively, this proves the robustness of the NH_4^+ -Orbitrap and the intensity-based relative
372 comparison between NH_4^+ -Orbitrap and two reference instruments. As previously reported, the Orbitrap
373 had a non-linear response to compounds present at extremely low concentrations, which was
374 independent of the sample composition, instrumental setup, or the reagent ion (Riva et al., 2020; Cai et
375 al., 2022). A similar evaluation was performed for the NH_4^+ -Orbitrap by comparing the measured versus
376 the theoretical isotopic intensities. As shown in Fig. S5, the NH_4^+ -Orbitrap had a linear response for ion
377 intensity greater than $\sim 5 \times 10^3$ cps, which corresponded to a limit of quantification (LoQ, corresponding
378 to the lowest normalized signal observed within the linear range) of $\sim 5 \times 10^5$ molecules cm^{-3} for OOMs,
379 estimated using the calibration factor derived from the NO_3^- -LTOF; which is consistent with a previous
380 study (Riva et al., 2020).

381 Figure 5 presents the concentrations of all OOMs measured by the NH_4^+ -Orbitrap determined by
382 applying two different calibration factors. The concentrations of OOMs measured by the NH_4^+ -Orbitrap
383 were higher than both the NO_3^- -LTOF and the PTR3-TOF which was optimized for measuring ammonia

and amines. This indicates that the NH_4^+ -Orbitrap can provide a better constraint on the concentrations of the primary products. As an example, pinonaldehyde (i.e., $\text{C}_{10}\text{H}_{16}\text{O}_2$), as one of the most abundant oxidation products, was not efficiently detected by the NO_3^- -LTOF, which is consistent with the higher selectivity of the NO_3^- reagent ion. To further illustrate the selectivity of the different reagent ions, Fig. 6 offers a summary of the performance of each mass spectrometer in detecting monomeric compounds, such as $\text{C}_{10}\text{H}_{16}\text{O}_n$. The y-axis is arbitrary and represents a qualitative characterization of the oxygen content when compounds were detected by different CI schemes. Similar to previous results, the I^- -CIMS detected OOMs with $n_{\text{O}} > 3$, but was not optimal for the detection of monomers with $n_{\text{O}} > 7$ (Riva et al., 2019b). The NO_3^- -LTOF was mainly selective towards HOMs with $n_{\text{O}} > 6$ (Riva et al., 2019b). The PTR3-TOF had limited capabilities in detecting OOMs with $n_{\text{O}} > 5$ due to the optimization of the instrument to obtain a very sensitive measurement of ammonia. Previously, the amine-CI demonstrated promise for the detection of OOMs, but was limited to applications with comparatively clean conditions due to considerable depletion of the reagent ion and the presence of overlapping peaks (Berndt et al., 2018b; Riva et al., 2019b). While showing a similar OOMs detection range to amine-CI, NH_4^+ -CI in tandem with the greater mass resolving power of the Orbitrap mass analyzer provided a linear response to higher loading. As shown in Fig. S6, background peaks were not affected by atmospherically relevant concentrations of O_3 and α -pinene. Overall, the NH_4^+ -Orbitrap appears to have the potential for providing a more reliable identification/quantification of OOMs produced from VOC oxidation compared to other existing mass spectrometry techniques.

3.5 Volatility distribution by four instruments

Figure 7 shows the distribution of oxidation products measured by four MS instruments according to their saturation vapor concentrations ($\log_{10}C_{\text{sat}}$) estimated using the modified Li et al. approach (Li et al., 2016; Isaacman-Vanwertz and Aumont, 2021). OOMs were grouped into six volatility regimes based on a volatility basis set (VBS): ultra-low volatility (ULVOCs); extremely low volatility (ELVOCs); low-volatility (LVOCs); semi-volatile (SVOCs); intermediate volatility organic compounds (IVOC); and VOC. ULVOCs and ELVOCs initiate cluster growth and form new particles. The total signal in each volatility bin represented the sum of the signal intensity of OOMs within the volatility range. The mean contributions of these compound regimes are shown in the VBS pie charts. The ULVOC, ELVOC, and LVOC regimes were well captured by NH_4^+ -Orbitrap and NO_3^- -LTOF. The PTR3-TOF only characterized the SVOC and IVOC regime (along with VOCs). IVOC and VOC regimes in the PTR3-TOF and NH_4^+ -Orbitrap were generally less oxygenated VOCs (i.e., $n_{\text{O}} < 5$). IVOC comprised the biggest mass contributions for the NH_4^+ -Orbitrap, and LVOC dominated in the NO_3^- -LTOF. Hence, the detection of the NH_4^+ -Orbitrap covered the widest range of volatilities, clearly highlighting the benefit of using this technique for the formation and fate of OOMs. In the past, reagent switching has not been practical, and users would run multiple mass spectrometer systems in parallel or use a Multi-scheme chemical IONization inlet (MION) with only one mass spectrometer to obtain the fullest possible mass spectrum (Rissanen et al., 2019; Huang et al., 2021). With NH_4^+ -Orbitrap it is now possible to cover the entire range of compounds which was not the case with most CI techniques.

422 **3.6 RH dependance of NH₄⁺-Orbitrap**

423 The sensitivity of the reagent-adduct ionization has been reported to be affected by the presence of water
424 vapor for a variety of reagent ions (Lee et al., 2014; Breitenlechner et al., 2017). The impact of RH on
425 the detection of OOMs by the NH₄⁺-Orbitrap was also studied. While the concentrations of gas phase
426 precursor and oxidant remained constant, the RH was raised from 10% to 80%. During this increase the
427 signal of organic vapor behaved inconsistently under an otherwise constant gas-phase production rate
428 (Surdu et al., 2023) and an increase in the condensation sink (Fig. S7). As shown in Fig. 8, the NH₄⁺-
429 Orbitrap demonstrated an RH dependence. For instance, the signal of less oxygenated molecules (i.e.,
430 $n_O < 5$) increased with increasing RH, especially compounds with $n_C = 8$; while the signal of highly
431 oxygenated molecules (i.e., $n_O > 10$) decreased as a function of RH. The average behavior of all C₈₋₁₀
432 monomers and C₁₈₋₂₀ dimers was summarized and compared between four instruments (Fig. S8). The
433 other three mass spectrometers also showed obvious RH dependence. Similar to NH₄⁺-Orbitrap, OOMs
434 with $n_O < 5$ measured by NO₃⁻-LTOF and PTR3-TOF increased at high RH, and a reverse tendency for
435 HOMs with $n_O > 11$, while OOMs with $n_O = 8\sim11$ seemed to be independent to RH. The large variations
436 of OOMs intensity at different RH measured by NH₄⁺-Orbitrap may be due to the widest range of oxygen
437 atoms. The causes why OOMs with different oxygen numbers measured by four instruments changed
438 with RH was not clear. Here, multiple possible reasons were provided to explain the signal evolution of
439 the ions with changing RH, such as water affecting the ionization efficiency or altering the
440 physicochemical processes of the gas phase chemistry.

441 First, the efficiency of a particular compound partly relied on whether water vapor competes with
442 the ammonium ion, lowering the sensitivity, or whether it acted as a third body to stabilize the
443 ammonium-organic analyte cluster by removing extra energy from the collision, raising the sensitivity
444 (Lee et al., 2014). NH₄⁺ primary ions can cluster with water molecules when humidity increased, thereby
445 reducing the clustering of the NH₄⁺ with organic analytes (Breitenlechner et al., 2017). However, the
446 formed NH₄⁺X_n (X being NH₃ or H₂O; n = 1,2) clusters might also act as reagent ions and ionize OOMs
447 through ligand switching reactions, which were expected to be fast and thus improve the charging
448 efficiency (Hansel et al., 2018). Compared to previous NH₄⁺-CIMS, the NH₄⁺X_n reagent ions were
449 expected to be larger due to the absence of the field in the ion-molecular-reaction zone in Orbitrap,
450 resulting in greater ligand exchanging and increasing the sensitivity for the less oxygenated species
451 (Canaval et al., 2019).

452 For RH-independent compounds, this may be due to the existence of very stable complexes with
453 NH₄⁺ reagent ion, or sufficient internal vibrational modes to disperse extra energy from the collision
454 (Lee et al., 2014). The highly oxygenated dimers in the category of ULVOCs and ELVOCs which
455 largely partition to the particle phase regardless of the presence of water might indicate that water may
456 also affect the physicochemical processes (i.e., multiphase chemistry, partitioning, etc.), in this case
457 possibly leading to an increase in the driving force of gas-particle partitioning of highly oxygenated
458 species (Surdu et al., 2023), and/or causing the decomposition of highly oxygenated molecules in the
459 particle phase to create less and moderately oxygenated products, e.g., C₈H₁₂O₁₋₅ (up to a 30-fold

460 increase in the gas phase) (Pospisilova et al., 2020), although which in the range of SVOCs (e.g.,
461 C₈H₁₂O_{4,5}) was also thought to partition more to the particle phase at higher RH (Surdu et al., 2023).
462 Finally, while water vapor could affect the gas-phase chemistry through water reactions with the Criegee
463 intermediates (CIs), HO₂ chemistry, OH radical concentration, no clear evidence has been identified as
464 earlier discussed by Surdu et al (2023). However, the accurate reasons needs to be further verified in
465 target control experiments like changing the RH in IMR of CI inlet.

466 **4 Summary**

467 In conclusion, this study presented an intercomparison between NH₄⁺-Orbitrap, NO₃⁻-LTOF, PTR3-
468 TOF, and I⁻-CIMS based on the identification and quantification of OOMs formed from the ozonolysis
469 of α -pinene under various environmental conditions. We used NH₄⁺ adduct ions with the Orbitrap mass
470 spectrometer to measure the oxygenated species for the first time. NH₄⁺-Orbitrap is a promising CIMS
471 technique for a comprehensive measurement of the whole product distribution and provides a more
472 complete understanding of the molecular composition and volatility of OOMs. This allows NH₄⁺-
473 Orbitrap to better monitor the evolution of organic compounds, which can be beneficial for air quality,
474 pollutant transport, and climate models. It is worth expecting that NH₄⁺-Orbitrap can be not only useful
475 for laboratory-based studies but also to field observations, to provide a deeper understanding of
476 atmospheric oxidation processes. However, it remains challenging to accurately quantify the
477 concentrations of OOMs due to the absent signals of reagent ions. In addition, RH influences NH₄⁺-
478 Orbitrap sensitivity, which can be different for each OOM. Therefore, this specific effect requires more
479 attention and dedicated studies before that the NH₄⁺-Orbitrap can be used in field studies, for example,
480 injection of pure or mixture of standards in atmospheric chamber at varying RH. From what is presented
481 here, the understanding of RH effect on the NH₄⁺-Orbitrap capabilities is too scarce to be able to
482 understand the time series evolution of OOMs that would be obtained in the real atmosphere.

483 **Conflicts of interest**

484 There are no conflicts to declare.

485 **Acknowledgements**

486 We thank the European Organization for Nuclear Research (CERN) for supporting CLOUD with
487 important technical and financial resources. We thank the Orbitool team for developing the tools to
488 analyze mass spectra. This work was financially supported by the French National program LEFE (Les
489 Enveloppes Fluides et l'Environnement), the European Research Council (ERC-StG MAARvEL; no.
490 852161), the European Union's Horizon 2020 research and innovation programme (Marie Skłodowska-
491 Curie grant agreement no. 764991 and 701647), the Swiss National Science Foundation (no.
492 200021_169090, 200020_172602, 20FI20_172622, and 206021_198140), the US National Science
493 Foundation (NSF_AGS_1801280, NSF_AGC_1801574, NSF_AGS_1801897, NSF_AGS_2132089),
494 and the German Federal Ministry of Education and Research (CLOUD-16 01LK1601A). D.D.L. thanks
495 the China Scholarship Council of P. R. China for the Ph.D. grant. M.Y.W. acknowledges financial
496 support from the Schmidt Science Fellows Program by Schmidt Futures, in partnership with the Rhodes
497 Trust.

498 **Author Contributions**

499 D.D.L., D.Y.W., L.C., W.S., M.Y.W., S.T., G.M., M.S., E.E., X.D.G., L.G.-C., M.G., J.P., B.R., B.S.,
500 P.R., S.P., A.H., J.C., J.K., N.M.D., C.G., I.E.-H., and M.R. prepared the CLOUD facility or measuring
501 instruments. D.D.L., D.Y.W., L.C., W.S., M.Y.W., S.T., G.M., M.S., E.E., X.D.G., L.G.-C., M.G., J.P.,
502 B.R., B.S., J.K., and M.R. collected the CLOUD data. D.D.L., D.Y.W., L.C., W.S., M.Y.W., G.M., and
503 M.R. and analysed the data. D.D.L., D.Y.W., M.Y.W., N.M.D., C.G., I.E.-H., and M.R. wrote the
504 manuscript and contributed to the scientific discussion. All authors discussed the results and commented
505 on the paper.

506 **References**

507 Berndt, T., Mentler, B., Scholz, W., Fischer, L., Herrmann, H., Kulmala, M., and Hansel, A.: Accretion
508 Product Formation from Ozonolysis and OH Radical Reaction of α -Pinene: Mechanistic Insight and the
509 Influence of Isoprene and Ethylene, *Environmental Science & Technology*, 52, 11069-11077,
510 10.1021/acs.est.8b02210, 2018a.

511 Berndt, T., Scholz, W., Mentler, B., Fischer, L., Herrmann, H., Kulmala, M., and Hansel, A.: Accretion
512 Product Formation from Self- and Cross-Reactions of RO₂ Radicals in the Atmosphere, *Angewandte
513 Chemie International Edition*, 57, 3820-3824, 10.1002/anie.201710989, 2018b.

514 Bianchi, F., Kurtén, T., Riva, M., Mohr, C., Rissanen, M. P., Roldin, P., Berndt, T., Crounse, J. D.,
515 Wennberg, P. O., Mentel, T. F., Wildt, J., Junninen, H., Jokinen, T., Kulmala, M., Worsnop, D. R.,
516 Thornton, J. A., Donahue, N., Kjaergaard, H. G., and Ehn, M.: Highly Oxygenated Organic Molecules
517 (HOM) from Gas-Phase Autoxidation Involving Peroxy Radicals: A Key Contributor to Atmospheric
518 Aerosol, *Chemical Reviews*, 119, 3472-3509, 10.1021/acs.chemrev.8b00395, 2019.

519 Bianchi, F., Tröstl, J., Junninen, H., Frege, C., Henne, S., Hoyle, C. R., Molteni, U., Herrmann, E.,
520 Adamov, A., Bukowiecki, N., Chen, X., Duplissy, J., Gysel, M., Hutterli, M., Kangasluoma, J.,
521 Kontkanen, J., Kürten, A., Manninen, H. E., Münch, S., Peräkylä, O., Petäjä, T., Rondo, L., Williamson,
522 C., Weingartner, E., Curtius, J., Worsnop, D. R., Kulmala, M., Dommen, J., and Baltensperger, U.: New
523 particle formation in the free troposphere: A question of chemistry and timing, *Science*, 352, 1109-1112,
524 10.1126/science.aad5456, 2016.

525 Breitenlechner, M., Fischer, L., Hainer, M., Heinritzi, M., Curtius, J., and Hansel, A.: PTR3: An
526 Instrument for Studying the Lifecycle of Reactive Organic Carbon in the Atmosphere, *Analytical
527 Chemistry*, 89, 5824-5831, 10.1021/acs.analchem.6b05110, 2017.

528 Cai, R., Huang, W., Meder, M., Bourgain, F., Aizikov, K., Riva, M., Bianchi, F., and Ehn, M.: Improving
529 the Sensitivity of Fourier Transform Mass Spectrometer (Orbitrap) for Online Measurements of
530 Atmospheric Vapors, *Analytical Chemistry*, 94, 15746-15753, 10.1021/acs.analchem.2c03403, 2022.

531 Cai, R., Li, Y., Clément, Y., Li, D., Dubois, C., Fabre, M., Besson, L., Perrier, S., George, C., Ehn, M.,
532 Huang, C., Yi, P., Ma, Y., and Riva, M.: Orbitool: a software tool for analyzing online Orbitrap mass

533 spectrometry data, *Atmospheric Measurement Techniques*, 14, 2377-2387, 10.5194/amt-14-2377-2021,
534 2021.

535 Canaval, E., Hyttinen, N., Schmidbauer, B., Fischer, L., and Hansel, A.: NH_4^+ Association and Proton
536 Transfer Reactions With a Series of Organic Molecules, *Frontiers in Chemistry*, 7,
537 10.3389/fchem.2019.00191, 2019.

538 Caudillo, L., Rörup, B., Heinritzi, M., Marie, G., Simon, M., Wagner, A. C., Müller, T., Granzin, M.,
539 Amorim, A., Ataei, F., Baalbaki, R., Bertozzi, B., Brasseur, Z., Chiu, R., Chu, B., Dada, L., Duplissy,
540 J., Finkenzeller, H., Gonzalez Carracedo, L., He, X. C., Hofbauer, V., Kong, W., Lamkaddam, H., Lee,
541 C. P., Lopez, B., Mahfouz, N. G. A., Makhmutov, V., Manninen, H. E., Marten, R., Massabò, D.,
542 Mauldin, R. L., Mentler, B., Molteni, U., Onnela, A., Pfeifer, J., Philippov, M., Piedehierro, A. A.,
543 Schervish, M., Scholz, W., Schulze, B., Shen, J., Stolzenburg, D., Stozhkov, Y., Surdu, M., Tauber, C.,
544 Tham, Y. J., Tian, P., Tomé, A., Vogt, S., Wang, M., Wang, D. S., Weber, S. K., Welti, A., Yonghong,
545 W., Yusheng, W., Zauner-Wieczorek, M., Baltensperger, U., El Haddad, I., Flagan, R. C., Hansel, A.,
546 Höhler, K., Kirkby, J., Kulmala, M., Lehtipalo, K., Möhler, O., Saathoff, H., Volkamer, R., Winkler, P.
547 M., Donahue, N. M., Kürten, A., and Curtius, J.: Chemical composition of nanoparticles from α -pinene
548 nucleation and the influence of isoprene and relative humidity at low temperature, *Atmospheric
549 Chemistry and Physics*, 21, 17099-17114, 10.5194/acp-21-17099-2021, 2021.

550 Daumit, K. E., Kessler, S. H., and Kroll, J. H.: Average chemical properties and potential formation
551 pathways of highly oxidized organic aerosol, *Faraday discussions*, 165, 181-202, 10.1039/c3fd00045a,
552 2013.

553 Donahue, N. M., Epstein, S. A., Pandis, S. N., and Robinson, A. L.: A two-dimensional volatility basis
554 set: 1. organic-aerosol mixing thermodynamics, *Atmospheric Chemistry and Physics*, 11, 3303-3318,
555 10.5194/acp-11-3303-2011, 2011.

556 Ehn, M., Junninen, H., Petäjä, T., Kurtén, T., Kerminen, V. M., Schobesberger, S., Manninen, H. E.,
557 Ortega, I. K., Vehkamäki, H., Kulmala, M., and Worsnop, D. R.: Composition and temporal behavior
558 of ambient ions in the boreal forest, *Atmospheric Chemistry and Physics*, 10, 8513-8530, 10.5194/acp-
559 10-8513-2010, 2010.

560 Ehn, M., Thornton, J. A., Kleist, E., Sipila, M., Junninen, H., Pullinen, I., Springer, M., Rubach, F.,
561 Tillmann, R., Lee, B., Lopez-Hilfiker, F., Andres, S., Acir, I. H., Rissanen, M., Jokinen, T.,
562 Schobesberger, S., Kangasluoma, J., Kontkanen, J., Nieminen, T., Kurten, T., Nielsen, L. B., Jorgensen,
563 S., Kjaergaard, H. G., Canagaratna, M., Maso, M. D., Berndt, T., Petaja, T., Wahner, A., Kerminen, V.
564 M., Kulmala, M., Worsnop, D. R., Wildt, J., and Mentel, T. F.: A large source of low-volatility
565 secondary organic aerosol, *Nature*, 506, 476-479, 10.1038/nature13032, 2014.

566 Fan, J., Wang, Y., Rosenfeld, D., and Liu, X.: Review of Aerosol–Cloud Interactions: Mechanisms,
567 Significance, and Challenges, *Journal of the Atmospheric Sciences*, 73, 4221-4252, 10.1175/jas-d-16-
568 0037.1, 2016.

569 Hallquist, M., Wenger, J. C., Baltensperger, U., Rudich, Y., Simpson, D., Claeys, M., Dommen, J.,
570 Donahue, N. M., George, C., Goldstein, A. H., Hamilton, J. F., Herrmann, H., Hoffmann, T., Iinuma, Y., Jang, M., Jenkin, M. E., Jimenez, J. L., Kiendler-Scharr, A., Maenhaut, W., McFiggans, G., Mentel, T. F., Monod, A., Prévôt, A. S. H., Seinfeld, J. H., Surratt, J. D., Szmigielski, R., and Wildt, J.: The formation, properties and impact of secondary organic aerosol: current and emerging issues, *Atmospheric Chemistry and Physics*, 9, 5155-5236, 10.5194/acp-9-5155-2009, 2009.

575 Hansel, A., Scholz, W., Mentler, B., Fischer, L., and Berndt, T.: Detection of RO₂ radicals and other
576 products from cyclohexene ozonolysis with NH₄⁺ and acetate chemical ionization mass spectrometry,
577 *Atmospheric Environment*, 186, 248-255, 10.1016/j.atmosenv.2018.04.023, 2018.

578 Haywood, J. and Boucher, O.: Estimates of the direct and indirect radiative forcing due to tropospheric
579 aerosols: A review, *Reviews of Geophysics*, 38, 513-543, 10.1029/1999rg000078, 2000.

580 Heinritzi, M., Simon, M., Steiner, G., Wagner, A. C., Kürten, A., Hansel, A., and Curtius, J.:
581 Characterization of the mass-dependent transmission efficiency of a CIMS, *Atmospheric Measurement
582 Techniques*, 9, 1449-1460, 10.5194/amt-9-1449-2016, 2016.

583 Huang, W., Li, H., Sarnela, N., Heikkinen, L., Tham, Y. J., Mikkilä, J., Thomas, S. J., Donahue, N. M.,
584 Kulmala, M., and Bianchi, F.: Measurement report: Molecular composition and volatility of gaseous
585 organic compounds in a boreal forest – from volatile organic compounds to highly oxygenated organic
586 molecules, *Atmospheric Chemistry and Physics*, 21, 8961-8977, 10.5194/acp-21-8961-2021, 2021.

587 Isaacman-VanWertz, G. and Aumont, B.: Impact of organic molecular structure on the estimation of
588 atmospherically relevant physicochemical parameters, *Atmospheric Chemistry and Physics*, 21, 6541-
589 6563, 10.5194/acp-21-6541-2021, 2021.

590 Jimenez, J. L., Canagaratna, M. R., Donahue, N. M., Prevot, A. S. H., Zhang, Q., Kroll, J. H., DeCarlo,
591 P. F., Allan, J. D., Coe, H., Ng, N. L., Aiken, A. C., Docherty, K. S., Ulbrich, I. M., Grieshop, A. P.,
592 Robinson, A. L., Duplissy, J., Smith, J. D., Wilson, K. R., Lanz, V. A., Hueglin, C., Sun, Y. L., Tian, J.,
593 Laaksonen, A., Raatikainen, T., Rautiainen, J., Vaattovaara, P., Ehn, M., Kulmala, M., Tomlinson, J.
594 M., Collins, D. R., Cubison, M. J., Dunlea, J., Huffman, J. A., Onasch, T. B., Alfarra, M. R., Williams,
595 P. I., Bower, K., Kondo, Y., Schneider, J., Drewnick, F., Borrmann, S., Weimer, S., Demerjian, K.,
596 Salcedo, D., Cottrell, L., Griffin, R., Takami, A., Miyoshi, T., Hatakeyama, S., Shimono, A., Sun, J. Y.,
597 Zhang, Y. M., Dzepina, K., Kimmel, J. R., Sueper, D., Jayne, J. T., Herndon, S. C., Trimborn, A. M.,
598 Williams, L. R., Wood, E. C., Middlebrook, A. M., Kolb, C. E., Baltensperger, U., and Worsnop, D. R.:
599 Evolution of Organic Aerosols in the Atmosphere, *Science*, 326, 1525-1529,
600 doi:10.1126/science.1180353, 2009.

601 Jokinen, T., Sipilä, M., Junninen, H., Ehn, M., Lönn, G., Hakala, J., Petäjä, T., Mauldin, R. L., Kulmala,
602 M., and Worsnop, D. R.: Atmospheric sulphuric acid and neutral cluster measurements using CI-APi-
603 TOF, *Atmospheric Chemistry and Physics*, 12, 4117-4125, 10.5194/acp-12-4117-2012, 2012.

604 Kirkby, J., Duplissy, J., Sengupta, K., Frege, C., Gordon, H., Williamson, C., Heinritzi, M., Simon, M.,
605 Yan, C., Almeida, J., Tröstl, J., Nieminen, T., Ortega, I. K., Wagner, R., Adamov, A., Amorim, A.,

606 Bernhammer, A.-K., Bianchi, F., Breitenlechner, M., Brilke, S., Chen, X., Craven, J., Dias, A., Ehrhart,
607 S., Flagan, R. C., Franchin, A., Fuchs, C., Guida, R., Hakala, J., Hoyle, C. R., Jokinen, T., Junninen, H.,
608 Kangasluoma, J., Kim, J., Krapf, M., Kürten, A., Laaksonen, A., Lehtipalo, K., Makhmutov, V., Mathot,
609 S., Molteni, U., Onnela, A., Peräkylä, O., Piel, F., Petäjä, T., Praplan, A. P., Pringle, K., Rap, A.,
610 Richards, N. A. D., Riipinen, I., Rissanen, M. P., Rondo, L., Sarnela, N., Schobesberger, S., Scott, C.
611 E., Seinfeld, J. H., Sipilä, M., Steiner, G., Stozhkov, Y., Stratmann, F., Tomé, A., Virtanen, A., Vogel,
612 A. L., Wagner, A. C., Wagner, P. E., Weingartner, E., Wimmer, D., Winkler, P. M., Ye, P., Zhang, X.,
613 Hansel, A., Dommen, J., Donahue, N. M., Worsnop, D. R., Baltensperger, U., Kulmala, M., Carslaw,
614 K. S., and Curtius, J.: Ion-induced nucleation of pure biogenic particles, *Nature*, 533, 521,
615 10.1038/nature17953, 2016.

616 Lee, B. H., Lopez-Hilfiker, F. D., Mohr, C., Kurtén, T., Worsnop, D. R., and Thornton, J. A.: An Iodide-
617 Adduct High-Resolution Time-of-Flight Chemical-Ionization Mass Spectrometer: Application to
618 Atmospheric Inorganic and Organic Compounds, *Environmental Science & Technology*, 48, 6309-6317,
619 10.1021/es500362a, 2014.

620 Li, Y., Pöschl, U., and Shiraiwa, M.: Molecular corridors and parameterizations of volatility in the
621 chemical evolution of organic aerosols, *Atmospheric Chemistry and Physics*, 16, 3327-3344,
622 10.5194/acp-16-3327-2016, 2016.

623 Lopez-Hilfiker, F. D., Mohr, C., Ehn, M., Rubach, F., Kleist, E., Wildt, J., Mentel, T. F., Lutz, A.,
624 Hallquist, M., Worsnop, D., and Thornton, J. A.: A novel method for online analysis of gas and particle
625 composition: description and evaluation of a Filter Inlet for Gases and AEROSols (FIGAERO),
626 *Atmospheric Measurement Techniques*, 7, 983-1001, 10.5194/amt-7-983-2014, 2014.

627 Mellouki, A., Wallington, T. J., and Chen, J.: Atmospheric chemistry of oxygenated volatile organic
628 compounds: impacts on air quality and climate, *Chemical reviews*, 115, 3984-4014, 10.1021/cr500549n,
629 2015.

630 Mohr, C., Thornton, J. A., Heitto, A., Lopez-Hilfiker, F. D., Lutz, A., Riipinen, I., Hong, J., Donahue,
631 N. M., Hallquist, M., Petäjä, T., Kulmala, M., and Yli-Juuti, T.: Molecular identification of organic
632 vapors driving atmospheric nanoparticle growth, *Nature Communications*, 10, 10.1038/s41467-019-
633 12473-2, 2019.

634 Pospisilova, V., Lopez-Hilfiker, F. D., Bell, D. M., El Haddad, I., Mohr, C., Huang, W., Heikkinen, L.,
635 Xiao, M., Dommen, J., Prevot, A. S. H., Baltensperger, U., and Slowik, J. G.: On the fate of oxygenated
636 organic molecules in atmospheric aerosol particles, *Science Advances*, 6, eaax8922,
637 doi:10.1126/sciadv.aax8922, 2020.

638 Rissanen, M. P., Mikkilä, J., Iyer, S., and Hakala, J.: Multi-scheme chemical ionization inlet (MION)
639 for fast switching of reagent ion chemistry in atmospheric pressure chemical ionization mass
640 spectrometry (CIMS) applications, *Atmospheric Measurement Techniques*, 12, 6635-6646,
641 10.5194/amt-12-6635-2019, 2019.

642 Riva, M., Brüggemann, M., Li, D., Perrier, S., George, C., Herrmann, H., and Berndt, T.: Capability of
643 CI-Orbitrap for Gas-Phase Analysis in Atmospheric Chemistry: A Comparison with the CI-APi-TOF
644 Technique, *Analytical Chemistry*, 92, 8142-8150, 10.1021/acs.analchem.0c00111, 2020.

645 Riva, M., Ehn, M., Li, D., Tomaz, S., Bourgain, F., Perrier, S., and George, C.: CI-Orbitrap: An
646 Analytical Instrument To Study Atmospheric Reactive Organic Species, *Analytical Chemistry*, 91,
647 9419-9423, 10.1021/acs.analchem.9b02093, 2019a.

648 Riva, M., Rantala, P., Krechmer, J. E., Peräkylä, O., Zhang, Y., Heikkinen, L., Garmash, O., Yan, C.,
649 Kulmala, M., Worsnop, D., and Ehn, M.: Evaluating the performance of five different chemical
650 ionization techniques for detecting gaseous oxygenated organic species, *Atmospheric Measurement
651 Techniques*, 12, 2403-2421, 10.5194/amt-12-2403-2019, 2019b.

652 Schobesberger, S., Junninen, H., Bianchi, F., Lonn, G., Ehn, M., Lehtipalo, K., Dommen, J., Ehrhart, S.,
653 Ortega, I. K., Franchin, A., Nieminen, T., Riccobono, F., Hutterli, M., Duplissy, J., Almeida, J., Amorim,
654 A., Breitenlechner, M., Downard, A. J., Dunne, E. M., Flagan, R. C., Kajos, M., Keskinen, H., Kirkby,
655 J., Kupc, A., Kurten, A., Kurten, T., Laaksonen, A., Mathot, S., Onnela, A., Praplan, A. P., Rondo, L.,
656 Santos, F. D., Schallhart, S., Schnitzhofer, R., Sipila, M., Tome, A., Tsagkogeorgas, G., Vehkamaki, H.,
657 Wimmer, D., Baltensperger, U., Carslaw, K. S., Curtius, J., Hansel, A., Petaja, T., Kulmala, M.,
658 Donahue, N. M., and Worsnop, D. R.: Molecular understanding of atmospheric particle formation from
659 sulfuric acid and large oxidized organic molecules, *Proceedings of the National Academy of Sciences
660 of the United States of America*, 110, 17223-17228, 10.1073/pnas.1306973110, 2013.

661 Simon, M., Dada, L., Heinritzi, M., Scholz, W., Stolzenburg, D., Fischer, L., Wagner, A. C., Kürten, A.,
662 Rörup, B., He, X.-C., Almeida, J., Baalbaki, R., Baccarini, A., Bauer, P. S., Beck, L., Bergen, A.,
663 Bianchi, F., Bräkling, S., Brilke, S., Caudillo, L., Chen, D., Chu, B., Dias, A., Draper, D. C., Duplissy,
664 J., El-Haddad, I., Finkenzeller, H., Frege, C., Gonzalez-Carracedo, L., Gordon, H., Granzin, M., Hakala,
665 J., Hofbauer, V., Hoyle, C. R., Kim, C., Kong, W., Lamkaddam, H., Lee, C. P., Lehtipalo, K., Leiminger,
666 M., Mai, H., Manninen, H. E., Marie, G., Marten, R., Mentler, B., Molteni, U., Nichman, L., Nie, W.,
667 Ojdanic, A., Onnela, A., Partoll, E., Petäjä, T., Pfeifer, J., Philippov, M., Quéléver, L. L. J.,
668 Ranjithkumar, A., Rissanen, M. P., Schallhart, S., Schobesberger, S., Schuchmann, S., Shen, J., Sipilä,
669 M., Steiner, G., Stozhkov, Y., Tauber, C., Tham, Y. J., Tomé, A. R., Vazquez-Pufleau, M., Vogel, A.,
670 L., Wagner, R., Wang, M., Wang, D. S., Wang, Y., Weber, S. K., Wu, Y., Xiao, M., Yan, C., Ye, P.,
671 Ye, Q., Zauner-Wieczorek, M., Zhou, X., Baltensperger, U., Dommen, J., Flagan, R. C., Hansel, A.,
672 Kulmala, M., Volkamer, R., Winkler, P. M., Worsnop, D. R., Donahue, N. M., Kirkby, J., and Curtius,
673 J.: Molecular understanding of new-particle formation from α -pinene between -50 and $+25$ $^{\circ}$ C,
674 *Atmospheric Chemistry and Physics*, 20, 9183-9207, 10.5194/acp-20-9183-2020, 2020.

675 Stolzenburg, D., Fischer, L., Vogel, A. L., Heinritzi, M., Schervish, M., Simon, M., Wagner, A. C.,
676 Dada, L., Ahonen, L. R., Amorim, A., Baccarini, A., Bauer, P. S., Baumgartner, B., Bergen, A., Bianchi,
677 F., Breitenlechner, M., Brilke, S., Buenrostro Mazon, S., Chen, D., Dias, A., Draper, D. C., Duplissy, J.,
678 El Haddad, I., Finkenzeller, H., Frege, C., Fuchs, C., Garmash, O., Gordon, H., He, X., Helm, J.,
679 Hofbauer, V., Hoyle, C. R., Kim, C., Kirkby, J., Kontkanen, J., Kürten, A., Lampilahti, J., Lawler, M.,
680 Lehtipalo, K., Leiminger, M., Mai, H., Mathot, S., Mentler, B., Molteni, U., Nie, W., Nieminen, T.,

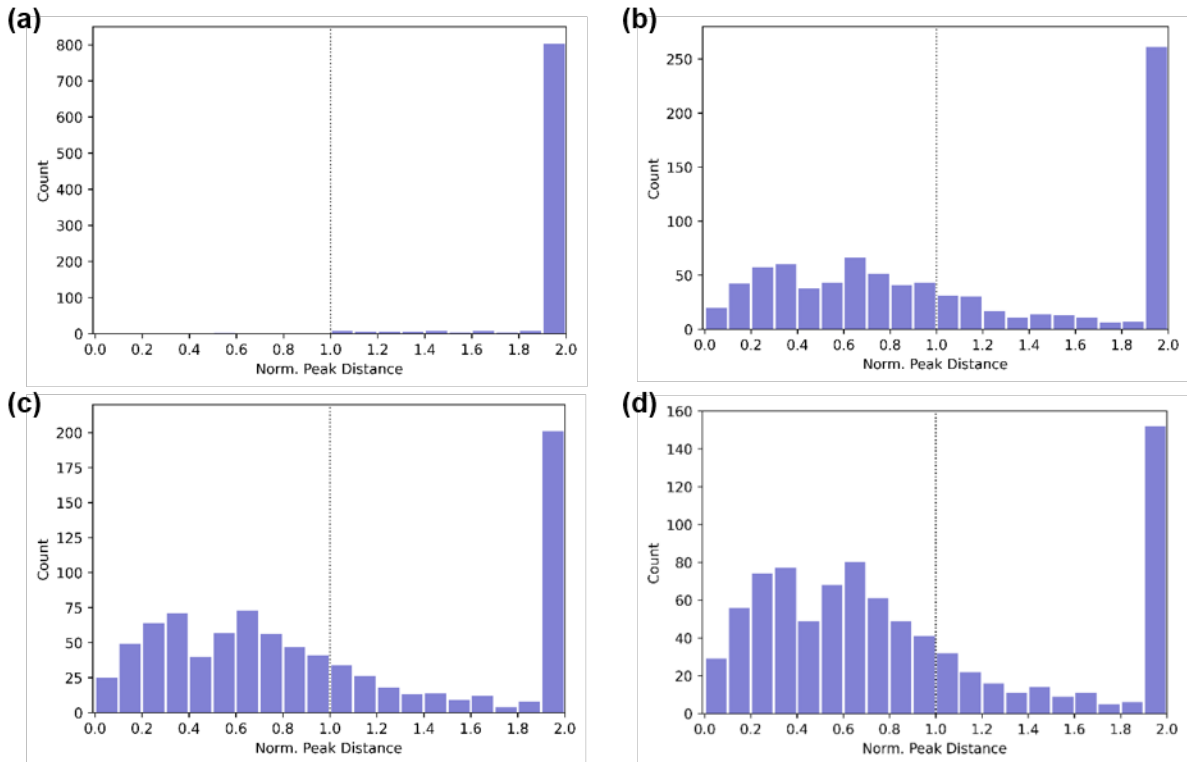
681 Nowak, J. B., Ojdanic, A., Onnela, A., Passananti, M., Petäjä, T., Quéléver, L. L. J., Rissanen, M. P.,
682 Sarnela, N., Schallhart, S., Tauber, C., Tomé, A., Wagner, R., Wang, M., Weitz, L., Wimmer, D., Xiao, M.,
683 Yan, C., Ye, P., Zha, Q., Baltensperger, U., Curtius, J., Dommen, J., Flagan, R. C., Kulmala, M.,
684 Smith, J. N., Worsnop, D. R., Hansel, A., Donahue, N. M., and Winkler, P. M.: Rapid growth of organic
685 aerosol nanoparticles over a wide tropospheric temperature range, *Proceedings of the National Academy
686 of Sciences*, 115, 9122-9127, 10.1073/pnas.1807604115, 2018.

687 Surdu, M., Lamkaddam, H., Wang, D. S., Bell, D. M., Xiao, M., Lee, C. P., Li, D., Caudillo, L., Marie,
688 G., Scholz, W., Wang, M., Lopez, B., Piedehierro, A. A., Ataei, F., Baalbaki, R., Bertozzi, B., Bogert,
689 P., Brasseur, Z., Dada, L., Duplissy, J., Finkenzeller, H., He, X.-C., Höhler, K., Korhonen, K., Krechmer,
690 J. E., Lehtipalo, K., Mahfouz, N. G. A., Manninen, H. E., Marten, R., Massabò, D., Mauldin, R., Petäjä,
691 T., Pfeifer, J., Philippov, M., Rörup, B., Simon, M., Shen, J., Umo, N. S., Vogel, F., Weber, S. K.,
692 Zauner-Wieczorek, M., Volkamer, R., Saathoff, H., Möhler, O., Kirkby, J., Worsnop, D. R., Kulmala,
693 M., Stratmann, F., Hansel, A., Curtius, J., Welti, A., Riva, M., Donahue, N. M., Baltensperger, U., and
694 El Haddad, I.: Molecular Understanding of the Enhancement in Organic Aerosol Mass at High Relative
695 Humidity, *Environmental Science & Technology*, 57, 2297-2309, 10.1021/acs.est.2c04587, 2023.

696 Viggiano, A. A., Seeley, J. V., Mundis, P. L., Williamson, J. S., and Morris, R. A.: Rate Constants for
697 the Reactions of $\text{XO}_3^-(\text{H}_2\text{O})_n$ (X = C, HC, and N) and $\text{NO}_3^-(\text{HNO}_3)_n$ with H_2SO_4 : Implications for
698 Atmospheric Detection of H_2SO_4 , *The Journal of Physical Chemistry A*, 101, 8275-8278,
699 10.1021/jp971768h, 1997.

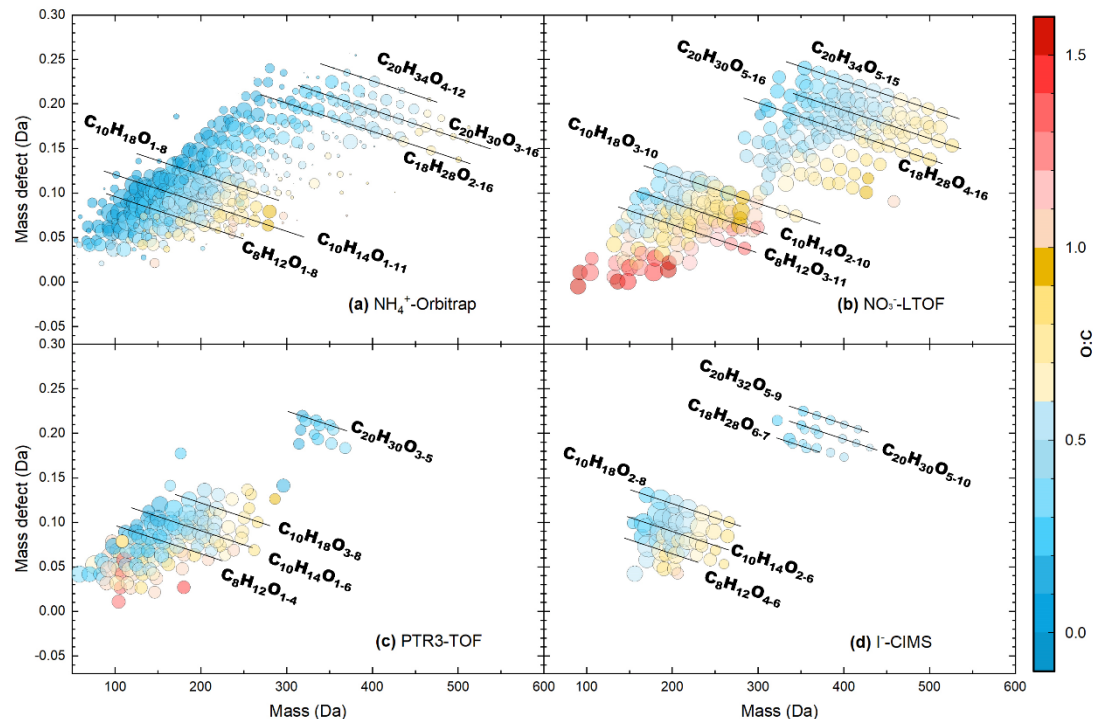
700 Wang, M., Kong, W., Marten, R., He, X.-C., Chen, D., Pfeifer, J., Heitto, A., Kontkanen, J., Dada, L.,
701 Kürten, A., Yli-Juuti, T., Manninen, H. E., Amanatidis, S., Amorim, A., Baalbaki, R., Baccarini, A.,
702 Bell, D. M., Bertozzi, B., Bräkling, S., Brilke, S., Murillo, L. C., Chiu, R., Chu, B., De Menezes, L.-P.,
703 Duplissy, J., Finkenzeller, H., Carracedo, L. G., Granzin, M., Guida, R., Hansel, A., Hofbauer, V.,
704 Krechmer, J., Lehtipalo, K., Lamkaddam, H., Lampimäki, M., Lee, C. P., Makhmutov, V., Marie, G.,
705 Mathot, S., Mauldin, R. L., Mentler, B., Müller, T., Onnela, A., Partoll, E., Petäjä, T., Philippov, M.,
706 Pospisilova, V., Ranjithkumar, A., Rissanen, M., Rörup, B., Scholz, W., Shen, J., Simon, M., Sipilä, M.,
707 Steiner, G., Stolzenburg, D., Tham, Y. J., Tomé, A., Wagner, A. C., Wang, D. S., Wang, Y., Weber, S.
708 K., Winkler, P. M., Wlasits, P. J., Wu, Y., Xiao, M., Ye, Q., Zauner-Wieczorek, M., Zhou, X., Volkamer,
709 R., Riipinen, I., Dommen, J., Curtius, J., Baltensperger, U., Kulmala, M., Worsnop, D. R., Kirkby, J.,
710 Seinfeld, J. H., El-Haddad, I., Flagan, R. C., and Donahue, N. M.: Rapid growth of new atmospheric
711 particles by nitric acid and ammonia condensation, *Nature*, 581, 184-189, 10.1038/s41586-020-2270-4,
712 2020.

713



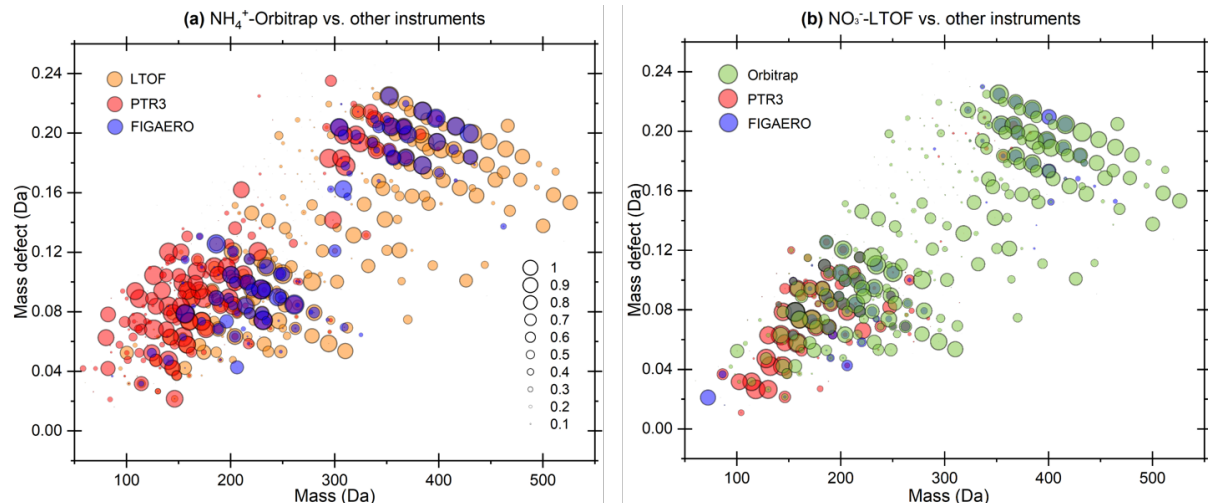
714

715 **Figure 1:** Number of adjacent peaks within a intensity threshold as the function of normalized peak
 716 distance observed by (a) NH₄⁺-Orbitrap and (b, c, d) NH₄⁺-TOF, respectively. The normalized peak
 717 distance was the ratio of distance between neighboring peaks to the full width at half maximum (FWHM).
 718 For each ion, the distance to the closest neighbor with a relative peak intensity that exceeded 20%, 50%,
 719 or 100% is recorded. (a) Orbitrap mass analyzer >99% of ions were separated by at least 1 FWHM from
 720 their neighbors with relative intensity threshold being set at 20%. (b) TOF mass analyzer (mass
 721 resolution ~10,000) >46% of ions were separated by at least 1 FWHM from their neighbors with a
 722 relative intensity threshold being set at 100%. (c) TOF mass analyzer >39% of ions were separated by
 723 at least 1 FWHM from their neighbors with a relative intensity threshold being set at 50%. (d) TOF mass
 724 analyzer >32% of ions were separated by at least 1 FWHM from their neighbors with a relative intensity
 725 threshold being set at 20%.



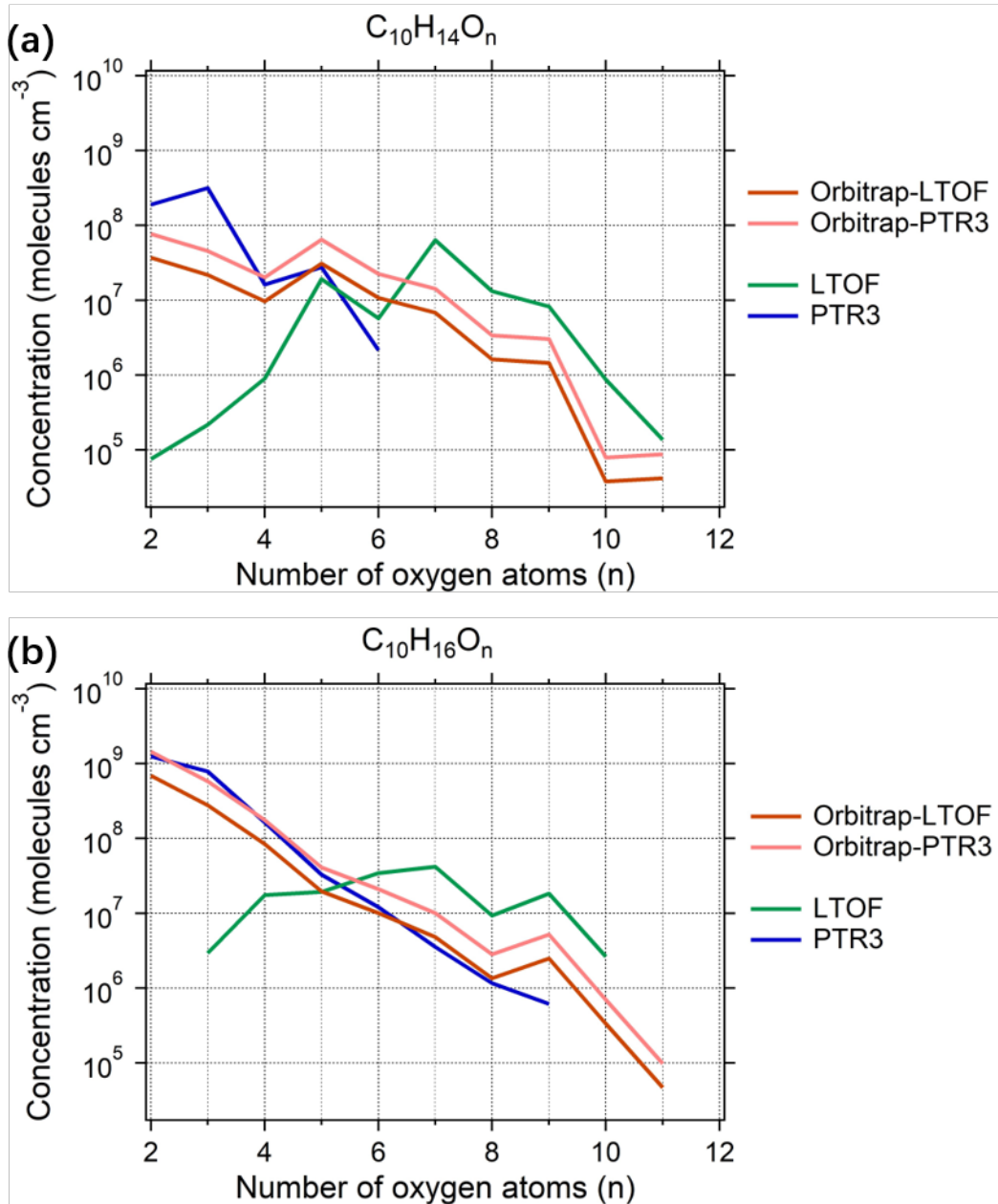
726

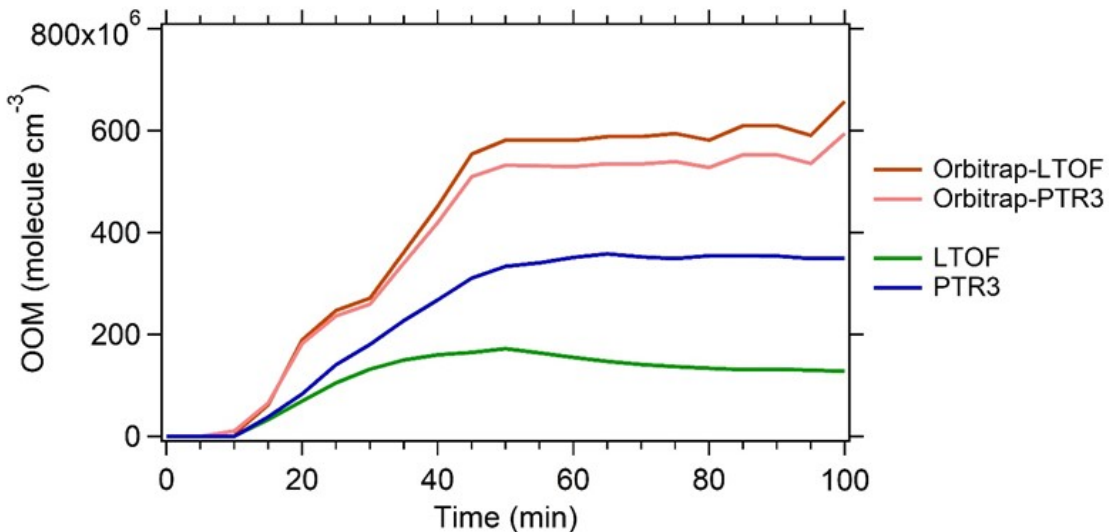
727 **Figure 2:** Mass defect plots for organic compounds measured by (a) NH_4^+ -Orbitrap, (b) NO_3^- -LTOF,
728 (c) PTR3-TOF and (d) I^- -CIMS in run 2211. The x-axis represents the mass-to-charge ratio of the neutral
729 analyte and the y-axis represents the corresponding mass defect, which is the difference between their
730 exact mass and nominal mass (Schobesberger et al., 2013). Markers were all sized by the logarithm of
731 their corresponding signals and colored by the O:C value. Some major OOMs measured by different
732 instruments were indicated by the black lines.



733

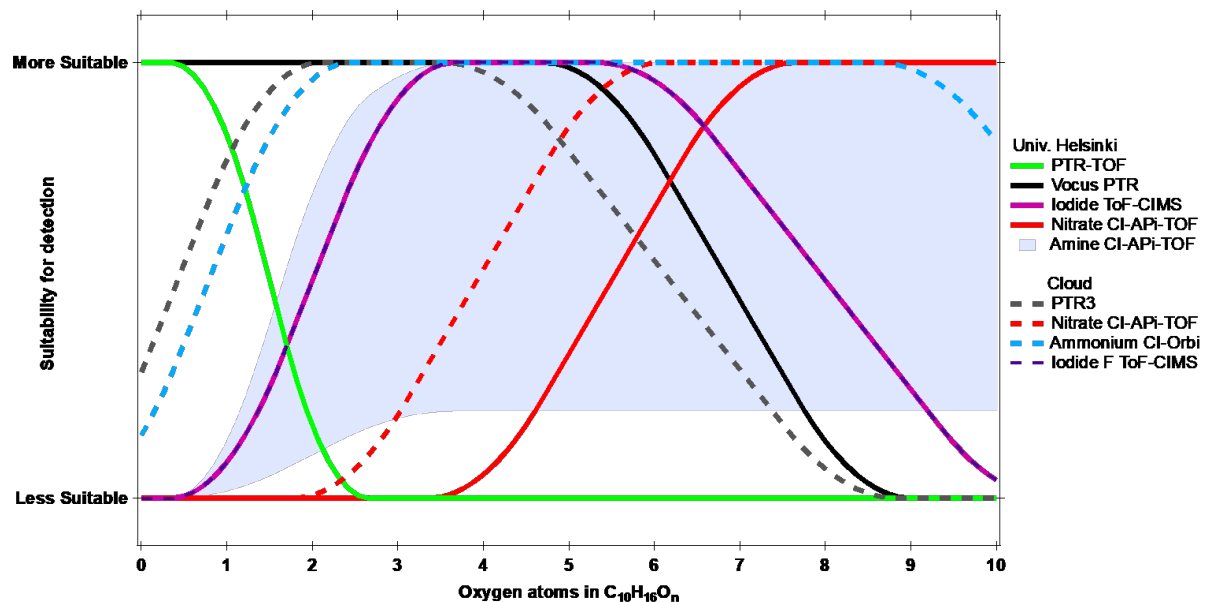
734 **Figure 3:** Mass defect plots depicting the compounds of which time series correlation was observed by
 735 (a) NH_4^+ -Orbitrap and (b) NO_3^- -LTOF with other MS instruments. Each circle represents a molecule
 736 and marker size represents the correlation R^2 of time series of the molecules between two different MS
 737 instruments. Two sets of data in run 2211 and 2213 were used to reduce uncertainties.





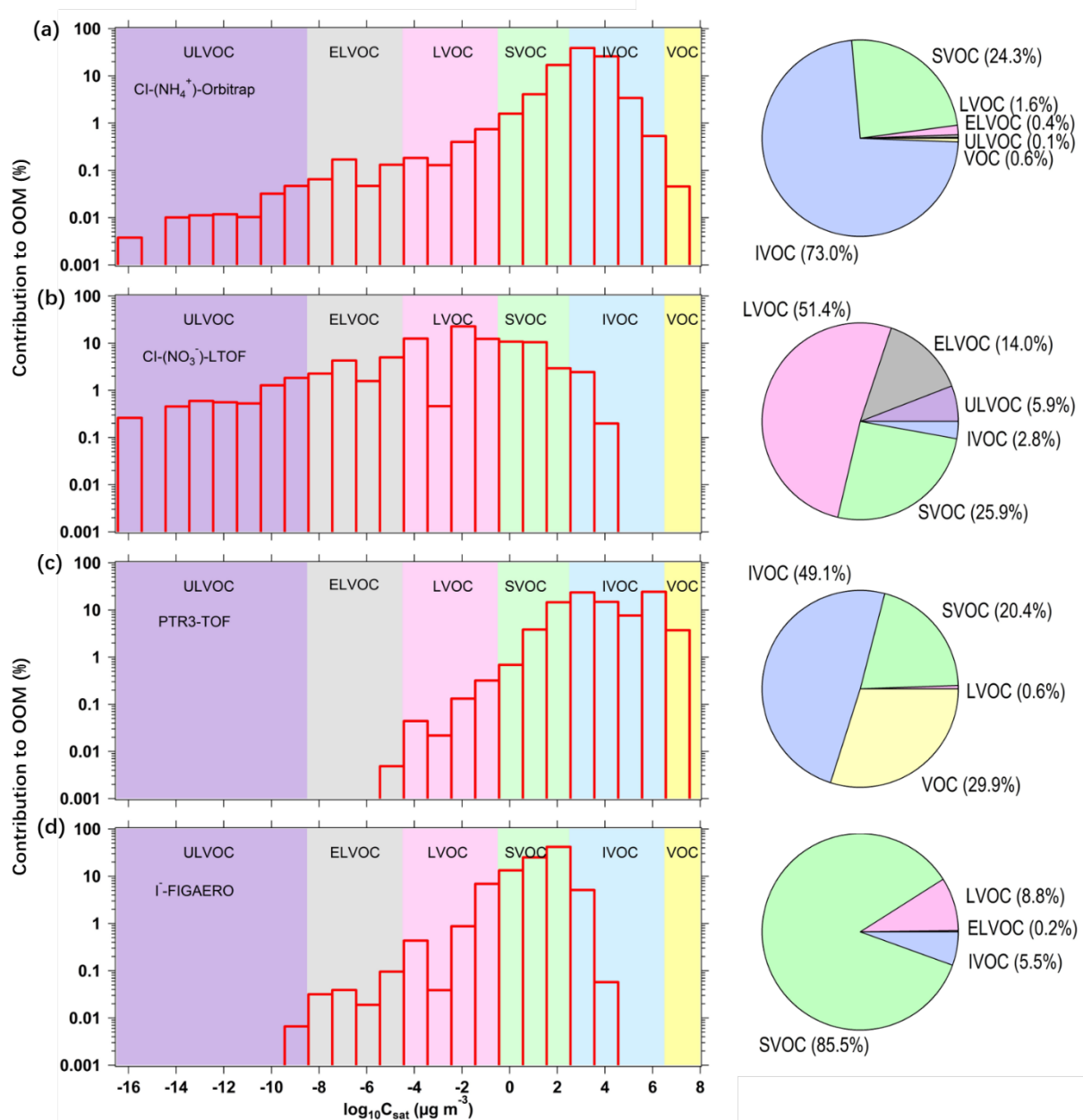
743

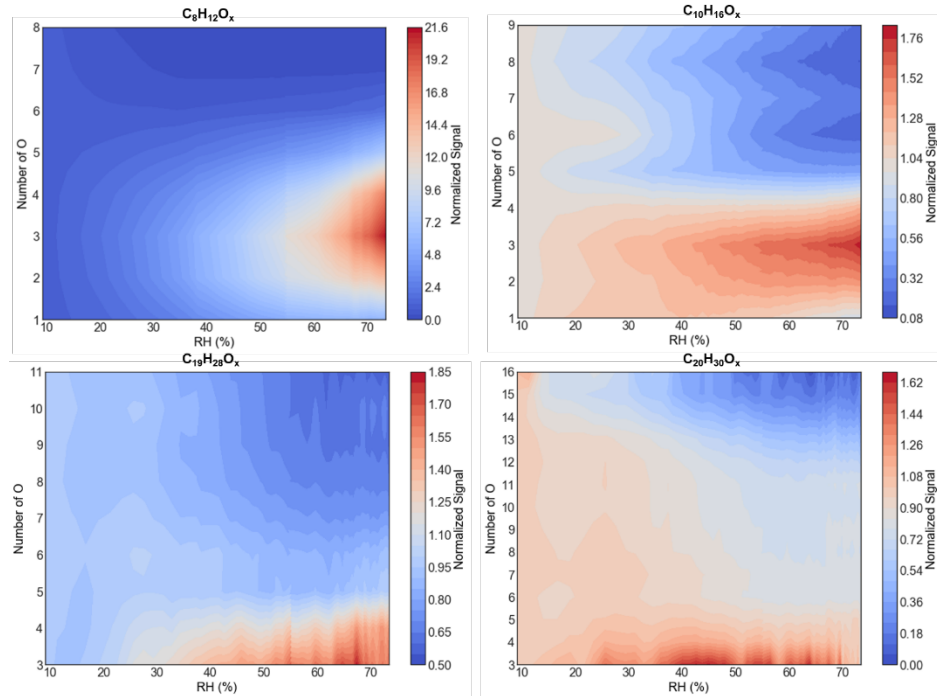
744 **Figure 5:** Estimated concentrations of all measured OOMs in the photooxidation of α -pinene. All
 745 monomers C_{8-10} and dimers C_{18-20} measured by NH_4^+ -Orbitrap, NO_3^- -LTOF, and PTR3-TOF in run 2213
 746 were summed up. The concentrations of OOMs measured by NH_4^+ -Orbitrap were quantified by the
 747 calibration factors derived from correlation analysis between NH_4^+ -Orbitrap and NO_3^- -LTOF (Orbitrap-
 748 LTOF, light green) or PTR3-TOF (Orbitrap-PTR3, light blue), respectively.



749

750 **Figure 6:** Estimated detection suitability of the different CIMS techniques for monomers from α -pinene
 751 ozonolysis, plotted as a function of the number of oxygen atoms. Image modified from Riva et al.(Riva
 752 et al., 2019b).





762

763 **Figure 8:** The effect of relative humidity on the distribution of the most abundant monomers and dimers
 764 measured by NH_4^+ -Orbitrap. The RH ramped from $\sim 10\%$ to $\sim 80\%$ in run 2211. The normalized signal
 765 represents the signal variation ratio at certain RH compared to that at RH = 10%, normalized signal =
 766
$$\frac{\text{signal}_{\text{RH}}}{\text{signal}_{10\%}}$$
.